JACS
JOURNAL OF THE AMERICAN CHEMICAL SOCIETY

Article

pubs.acs.org/JACS

# Hot Electron of Au Nanorods Activates the Electrocatalysis of Hydrogen Evolution on $MoS_2$ Nanosheets

Yi Shi, Jiong Wang, Chen Wang, Ting-Ting Zhai, Wen-Jing Bao, Jing-Juan Xu, Xing-Hua Xia,* and Hong-Yuan Chen

State Key Laboratory of Analytical Chemistry for Life Science and Collaborative Innovation Center of Chemistry for Life Sciences, School of Chemistry and Chemical Engineering, Nanjing University, 22 Hankou Road, Nanjing 210093, China

Supporting Information

**ABSTRACT:** Efficient water splitting through electrocatalysis holds great promise for producing hydrogen fuel in modern energy devices. Its real application however suffers from sluggish reaction kinetics due to the lack of high-performance catalysts except noble metals such as platinum. Herein, we report an active system of plasmonic-metal Au nanorods/molybdenum disulfide ($MoS_2$) nanosheets hybrids for the hydrogen evolution reaction (HER). The plasmonic Au−$MoS_2$ hybrids dramatically improve the HER, leading to a ∼3-fold increase of current under excitation of Au localized surface plasmon resonance (LSPR). A turnover of 8.76 $s^{-1}$ at 300 mV overpotential is measured under LSPR excitation, which by far exceeds the activity of $MoS_2$ catalysts reported recently. The HER enhancement can be largely attributed to the increase of carrier density in $MoS_2$ induced by the injection of hot electrons of Au nanorods. We demonstrate that the synergistic effect of the hole scavengers can further facilitate electron−hole separation, resulting in a decrease of the overpotential of HER at $MoS_2$ to ∼120 mV. This study highlights how metal LSPR activates the HER and promises novel opportunities for enhancing intrinsic activities of semiconducting materials.

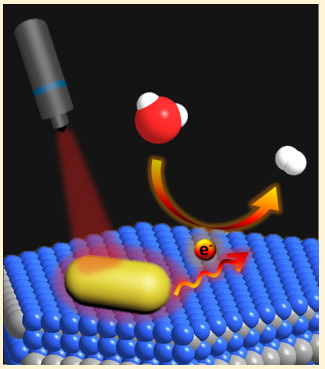


## INTRODUCTION

Hydrogen has been considered as the clean and renewable energy source of the next generation by virtue of its high energy density and environmentally friendly combustion product.[1,2] Electrochemically evolving hydrogen by splitting water is one of the most efficient and sustainable strategies for hydrogen generation. Up to date, hydrogen evolution can be easily achieved by electrolysis catalyzed by precious metals, such as Pt, Pd, and Rh.[3] The scarcity and high cost of these precious metals have seriously hampered their practical utilization. Nonprecious metal catalysts amenable for application in low-resource settings are ever in high demand. During the past few decades, various alternatives have been exploited, including enzyme, metal alloys, transition metal inorganic compounds, along with metal organic complexes.[4−8]

Theoretical and experimental studies have revealed that two-dimensional layered molybdenum disulfide ($MoS_2$) based materials would be the promising HER catalysts due to the optimal affinity of $H_2$ on the unsaturated sulfur atoms on the edges of $MoS_2$ nanosheets.[9,10] Density function theory (DFT) showed that the free energy of H adsorption on $MoS_2$ edge sites was neither too high nor too low ($\Delta G^{o}_{H} \cong 0$ eV).[10] The edges of $MoS_2$ were considered as active sites for $H_2$ evolution. The experimental results from Chorkendorff et al. suggested that electrocatalytic activity for HER correlated linearly with the number of edge sites on $MoS_2$ catalyst.[9] This conclusion was totally different from the observation on bulk $MoS_2$. As we know, pristine $MoS_2$ has poor electron transport property and requires very large overpotential to achieve considerable turnover frequencies of HER. Decreasing the overpotential of HER on $MoS_2$ based materials remains a significant challenge. To address this issue, tremendous strategies have been proposed to improve the catalytic activity of $MoS_2$ toward HER:[11−13] increasing the number of active sites, enhancing the intrinsic activity, and promoting the electron transport rate. Chemically exfoliated method is typically considered as an efficient pathway to produce active layered $MoS_2$ nanosheets (ce-$MoS_2$) in high yield. Due to violent nature of this reaction, the crystallinity of $MoS_2$ becomes seriously deformed, resulting in the phase conversion from stable semiconducting 2H-$MoS_2$ to ametastable metallic 1T-$MoS_2$. The ce-$MoS_2$ shows highly exposed edges and a decreased charge transfer resistance, which dramatically promotes the HER.[12] It has also been suggested that $MoS_2$ hybridized with metals and carbon materials can further improve the HER activity.[13−15] Although substantial progresses have been made, the research has only been focused on standalone electrocatalysis, and neglected the integrating of other driving forces such as photochemistry, especially the surface plasmon resonance (SPR) to the electrocatalysis systems.

SPR arises from the collective oscillation of conduction electrons of metal nanostructures and will excite high-energy electrons (referred to as "hot electrons") emerging on metal surface. When the plasmonic metallic nanostructures (such as Au, Ag, and Cu) are coupled to other substrates, for example,

**Received:** March 1, 2015
**Published:** May 28, 2015





DOI: 10.1021/jacs.5b01732
J. Am. Chem. Soc. 2015, 137, 7365−7370

the semiconductor (i.e., $TiO_2$, CdS, $WO_3$, graphene, $MoS_2$, $Fe_2O_3$), the plasmon-excited hot electrons can be injected from the metal nanoparticles into the conduction band of the semiconductors by overcoming the Schottky barrier.[16−21] It is demonstrated that plasmon-excited hot electrons can be injected into $MoS_2$ layer due to the low Schottky barrier between $MoS_2$ and Au and matched energy level.[22] In the photoelectrocatalytic water splitting system, semiconductors can provide trapping sites for the plasmon-excited electrons and suppress the electron−hole recombination, which promotes the water oxidation or reduction reaction on the semiconductors.[23] The plasmonic-metal/semiconductors system is of high and stable light harvesting efficiency, tunable absorption wavelength and lower electron−hole recombination rate, showing superiority over conventional cocatalyst/semiconductor systems using high energy ultraviolet light.[23] Due to outstanding light-trapping and electromagnetic-field concentrating properties of surface plasmon, charge carriers generated from plasmonic metal are formed near the semiconductor surface, which can reach the active sites more readily than that formed in the bulk.

We report herein a plasmon-activated HER electrochemical system of Au nanorods/$MoS_2$ nanosheets hybrids (Au−$MoS_2$). This system includes two essential components: (1) Au nanomaterial acting as a light absorber excites electron−hole pair during SPR process; (2) $MoS_2$ nanosheets acting as active sites and electron acceptor facilitate HER. By SPR excitation of Au nanostructure, hot electrons can be injected from Au into ce-$MoS_2$. This phenomenon results in an increase of charge density of ce-$MoS_2$ and, in turn, modulation of the energy level of the catalyst more comparable to HER. Thus, plasmons enhanced electrocatalytic activity for HER can be achieved.

## EXPERIMENTAL SECTION

**Reagents.** Molybdenum(IV) sulfide ($MoS_2$) powder and *n*-butyllithium in hexane (1.6 M) were purchased from Sigma-Aldrich. Hexadecyl trimethylammonium bromide (CTAB) and ascorbic acid (AA) were purchased from Johnson Matthey Corporation. $AgNO_3$, KCl, methanol, ethanol, ethylene glycol, and glycerol were purchased from Nanjing Chemical Reagent Co., Ltd. (Nanjing, China). $HAuCl_4 \cdot 4H_2O$ was purchased from the First Regent Factory (Shanghai, China). Glucose and sodium oleate (NaOL) were purchased from Sinopharm Chemical Reagent Co., Ltd. Fructose was purchased from Tokyo Chemical Industry Co., Ltd. All aqueous solutions were prepared with Millipore water (resistivity of 18.2 MΩ·cm). Indium−tin-oxide (ITO) glasses (≤10 Ω/sq) were purchased from Zhuhai Kaivo Optoelectronic Technology Co., Ltd.

**Fabrication of Gold Nanorods (NRs) with SPR Band Centered at ∼808 nm.** Gold NRs were fabricated according to the methods reported elsewhere.[24] Gold seeds solution was first prepared by adding 0.6 mL of ice-cold solution of 10 mM $NaBH_4$ to 10 mL of 0.25 mM $HAuCl_4$ prepared in 0.1 M CTAB solution under vigorous stirring for 2 min. The seeds were aged for 2 h in order to allow the hydrolysis of unreacted $NaBH_4$. The growth procedure was scaled up to obtain a 100 mL dispersion of gold NRs. Briefly, the solutions were added to a 250 mL conical flask, in the following order: 100 mL of 0.1 M CTAB solution, 1.0 mL of 10 mM silver nitrate solution, 2 mL of 25 mM aqueous $HAuCl_4$ and 0.2 mL of 1 M HCl solutions. To this mixed solution was added 0.70 mL of 0.0788 M AA as reducing agent, and the mixture was homogenized by stirring gently. Finally, a 120 μL of seed solution was added, and the whole solution was left undisturbed for about 14 h. Then, the as-synthesized gold NRs was centrifuged at 8000 rpm for 30 min in order to remove the unbound CTAB, the supernatant was discarded, and the precipitate was redispersed in 5 mL of Milli-Q water.

**Fabrication of Gold Nanorods (NRs) with SPR Band Centered at ∼650 nm.** Gold NRs were fabricated according to the methods reported elsewhere.[25] A total of 1.4 g of CTAB and 0.2468 g of NaOL were dissolved in 50 mL of warm water (∼50 °C). The solution was then cooled down to 30 °C and 50 mL of 1 mM $HAuCl_4$ was added, followed by addition of 2.4 mL of 4 mM $AgNO_3$. The resulting solution was kept undisturbed at 30 °C for 15 min and then stirred for 90 min at 700 rpm. Then, 0.42 mL of HCl (37 wt % in water) was added to adjust the pH. After stirring at 400 rpm for 15 min, 0.25 mL of 0.064 M ascorbic acid was added and the solution was vigorously stirred for 30 s. Finally, 0.16 mL of seed solution was injected into the solution. The resulting solution was stirred for 30 s and left undisturbed at 30 °C for 12 h. Similarly, the products were centrifuged at 8000 rpm for 30 min and the precipitate was redispersed in 10 mL of water. A 100 μL volume of the final solution was diluted to 10 mL with water for further surface modification.

**Fabrication of Chemically Exfoliated $MoS_2$ Nanosheets (ce-$MoS_2$).** The ce-$MoS_2$ was synthesized according to literature procedure.[26] Briefly, pristine bulk $MoS_2$ was intercalated with lithium by reacting $MoS_2$ powder (0.6 g) with *n*-butyl lithium in hexane (1.6 M, 6 mL) at 60 °C under argon atmosphere. After 2 days, the suspension was filtered over a 450 μm pore size membrane (Millipore) and washed with 60 mL of hexane for 3 times, giving a black powder of intercalated $MoS_2$ compound. Exfoliation was then immediately suspended in 30 mL of Millipore water and sonicated for 1 h. Exfoliated material was dialyzed for 5 days. The solution was centrifuged for several times to remove the unexfoliated materials. About 50 mL of supernatant was collected and used immediately.

**Fabrication of Gold NRs Modified Chemically Exfoliated $MoS_2$ (Au−$MoS_2$).** The Au−$MoS_2$ hybrid was prepared by mixing both the Au NRs and ce-$MoS_2$ solutions with a volume ratio of 2:5 (Supporting Information Scheme S1). Then, the mixture was sonicated for more than 1 h. Large amount of water was used to remove the excess of CTAB in the catalyst solution. In Supporting Information Figure S3D, the volume ratio of Au NRs and $MoS_2$ varies from 1:5 to 4:5.

**Structural Characterization.** UV−vis adsorption spectroscopic characterization was performed using a Nanodrop-2000C spectrophotometer (Thermo Fisher Scientific, Inc.). The morphologies of each sample were characterized by transmission electron microscopy (TEM, JEM-2100, Japan) by drying a droplet of sample solutions on Ni-grids with carbon film. Scanning electron microscopic (SEM) images were acquired on silicon wafers by S-4800 (Japan). Raman spectra were collected on a FT-Raman Spectrometer (Bruker). XPS spectra were obtained on a PHI 5000 VersaProbe (Japan). The binding energy was calibrated by means of the C 1s peak energy of 284.6 eV. The zeta potential measurements were performed with a Malvern Zetasizer Nano ZS90 analyzer at room temperature.

**HER Electrochemical Characterization.** All electrochemical measurements were carried out using a CHI 900D instrument (Chenhua, China) at 30 °C. A working electrode was made by drop-casting 10 μL of the catalyst to cover a glassy carbon electrode (3 mm diameter). A graphite rod was used as the counter electrode. An Ag/AgCl electrode was used as the reference for all the electrochemical tests, and the potential was calibrated to the reversible hydrogen electrode (RHE) for the tests of HER (the potential of the Ag/AgCl is 0.238 V versus RHE).

**Dark-Field Electrochemical Characterization.** Dark field images were acquired on a Nikon inverted microscope Eclipse Ti−U equipped with a colored CCD (Nikon, DS−FI1-U2). The surface plasmon resonance (SPR) scattering spectra were recorded using a SP2556 spectrograph mounted on the microscope, and a 512B_excelon EMCCD was used as the detector (Princeton Instruments). Glass slides were cleaned under PSD-UV4 ozone system (Novascan Technologies) before use. All tests were carried out at room temperature. The electrochemical apparatus is composed of three electrode with indium−tin-oxide glass (ITO) as the working electrode, a Pt wire as the auxiliary electrode, and Ag/AgCl as the reference. A 0.1 M KCl solution was used as the electrolyte.

**Modification of Au NRs on Glass Slide.** The Au NRs with SPR band centered at ∼650 nm were modified on ITO slide for dark field observation. Before modification, the microscope slide was sonicated


DOI: 10.1021/jacs.5b01732
J. Am. Chem. Soc. 2015, 137, 7365−7370

in acetone for 2 h to remove the dust particles. Then, the slide was thoroughly rinsed with water, blow-dried with nitrogen gas, and stepped by a treatment with Ultra-Violet/Ozone cleaner for 60 min to further remove the surface organic contaminants and make the glass hydrophilic. The cleaned slide was then immersed into the freshly prepared diluted Au NRs solution for 1 h; the positively charged Au NRs can be deposited on the negatively charged ITO via the electrostatic interaction. After successive rinsing with water and blow-drying with nitrogen gas, the Au/ITO was formed. Then, diluted ce-$MoS_2$ solution was dipped onto the Au/ITO (termed as Au−$MoS_2$/ITO) followed by successive rinsing with water and blow-drying with nitrogen gas.

**Gas Chromatography Characterization.** The photoelectrocatalytic reaction product of $H_2$ was measured using a Varian 3380 gas chromatograph equipped with a separation column (10% Carbowax 20 M + 5% KOH) and a thermal conductivity detector (TCD). Helium was used as the carrier gas in the chromatograph. The parameters were set as follows: column temperature (100 °C); injector temperature (120 °C); TCD temperature (150 °C); bridge current (180 mA).

## RESULTS AND DISCUSSION

Bulk $MoS_2$ was chemically exfoliated in aqueous solution, forming good-dispersible $MoS_2$ (ce-$MoS_2$) nanosheets. The SEM and TEM images of these materials and photograph of ce-$MoS_2$ aqueous solution refer to Supporting Information Figure S1A−C. Then, Au rods (Supporting Information Figure S1D) were assembled onto ce-$MoS_2$ through electrostatic interactions, forming Au−$MoS_2$ hybrids (Supporting Information Scheme S1). In our work, low loading of Au rods was used to avoid aggregation and plasmonic coupling of the loaded Au rods. TEM characterization (Figure 1A) of the hybrids reveals that Au rods are randomly decorated on the surface of ce-$MoS_2$ nanosheets. Optical characterizations reveal the existence of strong electronic interaction between Au and ce-$MoS_2$. The UV−vis spectrum of ce-$MoS_2$ exhibits the clear characteristic peaks in the near-UV range, while the one for Au rods shows a distinct SPR longitudinal band at 813 nm and a small transversal band at 515 nm. The spectrum of Au−$MoS_2$ displays the similar absorption bands of ce-$MoS_2$ and an obvious red-shifted SPR longitudinal band at 826 nm (Figure 1B), which indicates the electronic interactions between Au and semiconductor. The X-ray photoelectron spectroscopy (XPS) characterizations (Figure 1C−E) show that the binding energies of Mo 3d and S 2p in Au−$MoS_2$ are negatively shifted by ca. 0.60 and 0.27 eV, respectively, as compared to the ones for ce-$MoS_2$. The binding energy of Au 4f in Au−$MoS_2$ is positively shifted by ca. 0.29 eV compared to that of Au rods. These results confirm the electron transfer from Au to ce-$MoS_2$. The Au loading in Au−$MoS_2$ is calculated as 0.76 atom %, indicating trace quantity of Au in the hybrids. The XPS spectra for various samples (Au−$MoS_2$, ce-$MoS_2$, pristine $MoS_2$ and Au rod) and their corresponding atomic concentrations of Mo, S, and Au are shown in Supporting Information Figure S2. The effect of assembled Au rods on the electronic properties of ce-$MoS_2$ can be also revealed by Raman spectroscopy (Figure 1F). The $A_{1g}$ mode represents the out-of-plane lattice vibration with S atoms moving in the opposite directions.[27] The interaction between Au rods and $MoS_2$ stiffens the vertical vibration of S atoms,[28] resulting in a blue shift of the $A_{1g}$ mode by 2.43 $cm^{-1}$.

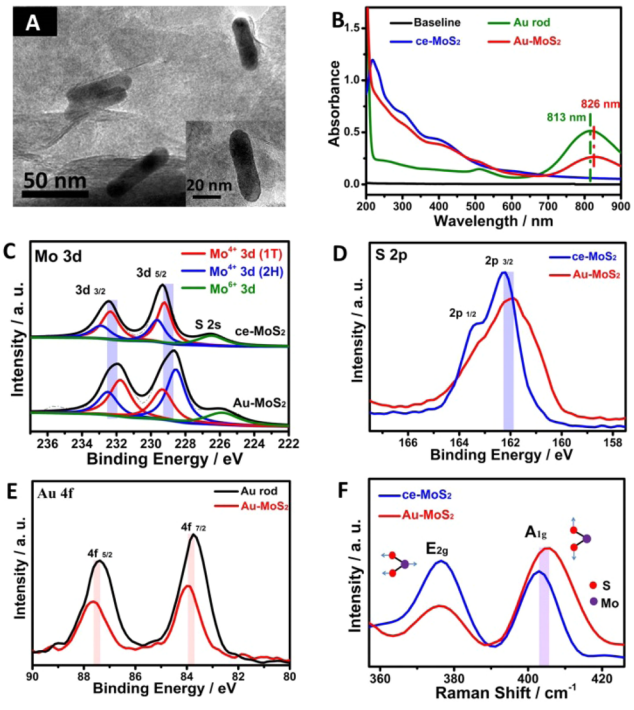


**Figure 1.** (A) TEM image of Au−$MoS_2$ hybrids. (B) UV−vis spectra of ce-$MoS_2$, Au rod and Au−$MoS_2$. XPS spectra of ce-$MoS_2$ and Au−$MoS_2$ in the Mo 3d (C), S 2p (D), and Au 4f (E) region. (F) Raman spectra of ce-$MoS_2$ and Au−$MoS_2$.

The electrocatalytic activity of the synthesized materials modified on glassy carbon electrodes toward HER was investigated in a $N_2$-saturated 0.5 M $H_2SO_4$ solution using a typical three-electrode configuration at 30 °C. As shown in Figure 2A, the bulk $MoS_2$ exhibits little HER activity. On the contrast, Au rods, ce-$MoS_2$ and Au−$MoS_2$ show different electrocatalytic activities toward HER, with onset potentials of −0.28, −0.25, and −0.22 V vs reversible hydrogen electrode (RHE), respectively. When irradiated with an 808 nm laser corresponding to the maximum LSPR absorption of Au rods, the HER activity of Au−$MoS_2$ is significantly improved, as evidenced by the positively shifted onset potential to −0.16 V

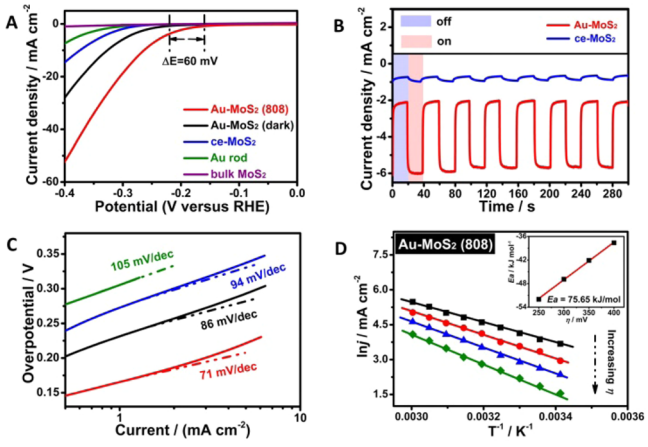


**Figure 2.** (A) HER polarization curves obtained on several catalysts as indicated. (B) $i$−$t$ curves with and without 808 nm laser excitation. (C) The Tafel plots of Au rod (green), ce-$MoS_2$ (blue), Au−$MoS_2$ (black), and Au−$MoS_2$ (808) (red) derived from the early stages of HER polarization curves. (D) Arrhenius plots: semilogarithmic dependence of current density at various overpotentials ($\eta$) plotted against inverse temperature ($T$). Overpotentials are taken from 250 to 400 mV at an interval of 50 mV. Inset: Activation energy at the zero overpotential obtained through trendextrapolation.



DOI: 10.1021/jacs.5b01732
J. Am. Chem. Soc. 2015, 137, 7365−7370

vs RHE. When the laser is removed at ca. −0.3 V, the polarization current (blue line) abruptly drops. Although it does not immediately return to the original state of Au−$MoS_2$ in the dark possible due to the thermal effect, the following potential scan shows the same polarization curve as the one in the dark (Supporting Information Figure S3A, compare the green and black curves). The photoelectrocatalytic product of $H_2$ by the plasmonic enhanced $MoS_2$ water splitter was measured using a gas chromatography (GC). The device was purged with $N_2$ for 1 h before each continuous gas-collecting operation. As indicated, the photoelectrocatalytic product with or without illumination shows the same GC peak position as that of the standard $H_2$ sample (Supporting Information Figure S4). Under the same conditions, the ce-$MoS_2$ modified electrode does not exhibit the obvious laser response observed in the case of Au−$MoS_2$ (Supporting Information Figure S3B). The slight increase in current could be due to the thermal effect since ce-$MoS_2$ weakly absorbs near-infrared light.[29] The $i$−$t$ curves of ce-$MoS_2$ and Au−$MoS_2$ at −0.23 V with and without 808 nm laser irradiation (1.5 W) are shown in Figure 2B. Initially, steady currents are observed without illumination. Upon 808 nm laser excitation, the current rapidly increases and immediately reaches the steady state. As the laser is switched off, the current returns to the initial value, showing good reversibility of the process. It is clear that the increased laser response current is considerably larger on Au−$MoS_2$ than ce-$MoS_2$, in consistence with the polarization curves (vide supra). Since the laser enhanced electrocatalytic activity toward HER is negligible under 532 and 650 nm laser irradiation where SPR absorption of Au rods does not appear (Supporting Information Figure S3C), we can ascribe the laser enhanced HER activity to the longitudinal SPR effect of Au rods via hot electrons injection into $MoS_2$. In addition, we also observe that the SPR enhanced electrocatalytic activity of Au−$MoS_2$ toward HER dramatically increases with increasing the laser intensity from 0.15 to 1.5 W and the loading density of Au rods (Supporting Information Figure S3C,D). This positive relationship between hot electron density and rate enhancement has been observed in photochemical water splitting half reaction.[23] Thus, we can also ascribe the observed SPR enhancement effect to the increased concentration of energetic hot electrons injected into the semiconductor with increase of laser intensity and Au rods loading density.

To better understand the rate-limiting step involved in HER, we performed Tafel plots (Figure 2C) to elucidate an inherent property of the catalysts. The HER mainly occurs via Volmer-Heyrovsky (Equations S1 and S2 in the Supporting Information) or Volmer−Tafel (Equations S1 and S3) mechanism.[13] When the adsorbed hydrogen coverage ($\Theta_H$) on catalysts is low, the Volmer reaction should possibly be the rate-limiting step with a theoretical Tafel slope of 120 mV/dec. For a high $\Theta_H$, a Heyrovsky or Tafel reaction should be usually the rate-determining step with a theoretical Tafel slope of 40 or 30 mV/dec, respectively. We observe that the three $MoS_2$ based catalysts show similar Tafel slopes, indicating similar reaction mechanism with the same rate-limiting step. The Tafel slope of bulk $MoS_2$ has been reported to be 692 mV/dec, which is considered to be an inefficient HER catalyst because of large internal resistance.[30] In our work, the Tafel slope of ce-$MoS_2$ is determined to be 94 mV/dec, which may be due to the presence of more active S edges and the higher charge transfer capability. After modification with Au rods, the Tafel slope becomes 86 mV/dec With 808 nm laser irradiation, the Au−$MoS_2$ hybrids exhibit a Tafel slope of 71 mV/dec. The decrease of Tafel slope indicates that the $\Theta_H$ on ce-$MoS_2$ based catalysts would be higher and the Volmer reaction is no longer the only step that influences the HER rate. The activation energy ($E_a$) at the zero overpotential for electrode reaction process is generally considered as an important feature to evaluate the performance of electrocatalysis at various materials in the same electrolyte. The value of $E_a$ for HER on ce-$MoS_2$ is calculated to be 94.82 kJ/mol (calculation details are shown in Supporting Information, Figure S5). After modification with Au rods and 808 nm laser irradiation, the value of $E_a$ for Au−$MoS_2$ decreases to 75.65 kJ/mol (Figure 2D), which indicates that the SPR effect can effectively lower the $E_a$ for HER. To gain more insights into the intrinsic catalytic activity, the turnover frequency (TOF) for the active sites was also measured (Supporting Information Figure S6). The efficient surface area of $MoS_2$ is determined by calculating the number of active sites from the "underpotential deposition (UPD) of copper" method (see details in Supporting Information).[31] The HER TOF for pure ce-$MoS_2$ is 1.2 $s^{-1}$. Due to the hot electrons injection, the TOF of Au−$MoS_2$ reaches 8.76 $s^{-1}$, which surpasses the various state-of-art $MoS_2$ reported recently (shown in Supporting Information Table S1).

It has been reported that the surface plasmons genereated hot electrons can be injected into the nearby electron acceptor.[23] We further employed dark-field microscopy to directly investigate the hot electron transfer process between Au and $MoS_2$ (apparatus shown in Supporting Information Photograph S1). In this study, Au rods (TEM image shown in Figure 3B, inset) with SPR peak centered at ∼650 nm

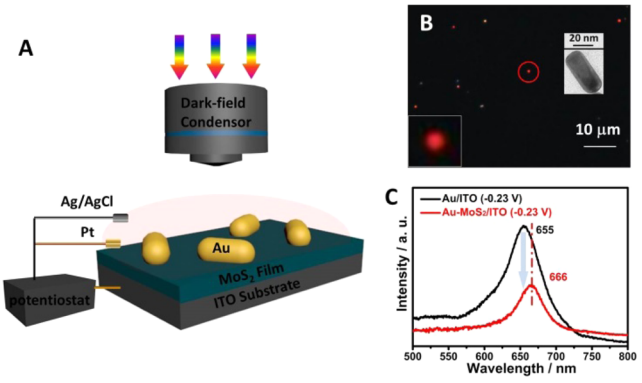


**Figure 3.** (A) Schematic apparatus for in situ electrochemical SPR scattering measurement in 0.1 M KCl solution under a dark-field microscope. The electrochemical cell consists of a Pt wire as the auxiliary electrode, an Ag/AgCl wire as the reference, and modified indium−tin-oxide (ITO) as the working electrode. (B) Dark-field image of Au rods deposited on ITO in 0.1 M KCl solution, scale bar = 10 $\mu$m. Inset shows the dark-field amplified image and TEM image of the labeled Au rods. (C) SPR scattering spectra of Au rods in Au/ITO and Au−$MoS_2$/ITO at −0.23 V vs RHE in 0.1 M KCl solution.

(Supporting Information Figure S7) were used due to the measuring range of our CCD detector lying only in the visible light. The *in situ* electrochemical SPR scattering spectroscopy is depicted in Figure 3A, which allows to collect the SPR spectrum of a single Au rod under applied potential. As shown in the dark-field image (Figure 3B), each spot exhibits red color, in approximately agreement with the UV−vis absorbance (Supporting Information Figure S7). We compare the SPR spectra of Au/ITO and Au−$MoS_2$/ITO at −0.23 V vs RHE. As


DOI: 10.1021/jacs.5b01732
J. Am. Chem. Soc. 2015, 137, 7365−7370

shown in Figure 3C, the SPR scattering of Au rods deposited on ITO is located at 655 nm. Further assembly of $MoS_2$ layer results in a red-shift of the LSPR scattering of Au rods to 666 nm, directly indicating that hot electron is exactly transferred from Au rods to $MoS_2$ nanosheets. This process generates a more efficient electron−hole separation state, which contributes to HER dramatically. The change of dielectric surrounding of Au rods due to the modification of $MoS_2$ may be another factor contributing to the red-shift of the LSPR. This electron transfer phenomenon is also observed at open circuit potential (refers to Supporting Information, Figures S8 and S9). It is worth noting that for Au−$MoS_2$/ITO, the scattering intensity is decreased by 56% as compared to that of pure Au rods, which may indicate the decreased ratio of scattering to absorption of the Au rods after $MoS_2$ modification.

On the basis of the above results, the expected mechanism of the enhanced activity of Au−$MoS_2$ toward HER under laser irradiation is shown in Figure 4. Upon laser excitation, surface

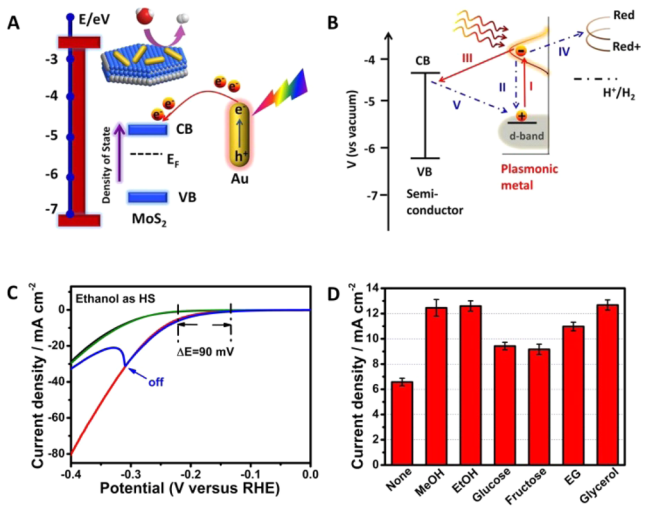


**Figure 4.** (A) Schematic Au−$MoS_2$ and energy level diagram illuminating hot electrons injection and change of $MoS_2$ Fermi level. (B) Different plausible hot electrons transfer pathways likely to occur during SPR. (C) Polarization curves of Au−$MoS_2$ under 808 nm laser irradiation with (red) or without (black) ethanol as HS. Green line represents the electrochemical behavior of Au−$MoS_2$ in the dark immediately after one irradiation cycle. Blue line represents the electrochemical behavior upon sudden light-off test. (D) Current density of Au−$MoS_2$ obtained from $i$−$t$ curves at −0.23 V under 808 nm laser excitation with a variety of scavenger chemicals. The concentrations of glucose and fructose solutions used were 25 wt %, whereas the rest were 10 vol %.

plasmons are proliferating near-field plasmonic waves at the interface between Au and ce-$MoS_2$, forming an electron−hole pair (process I). The generated energetic hot electrons will extend further away from the electron equilibrium state on Au rods and may have three probable transfer channels: (II) recombination with the hole in the metal; (III) injection into the CB of semiconductor; and (IV) direct electrochemical reduction of water on Au rods. Although we cannot exclude the existence of process IV, the contribution of this process to the enhanced photoelectrochemical current is negligible, since Au is not a good HER catalyst due to low $\Theta_H$, which is evidenced by the electrochemical result in Figure (2A, green curve). Low Schottky barrier exists between Au and $MoS_2$,[22] resulting in a faster electron injection from Au to $MoS_2$ (process III). The electron relaxation parallels the injection process simultaneously. Then, the injected hot electrons in CB of $MoS_2$ may be transferred to the electron-deficient Au, returning to its ground state (process V). The continuous hot electrons injection gives birth to a dynamic charge-separated state, with the electrons at the bottom of the ce-$MoS_2$ CB and the holes near the Au rod Fermi level. Due to the electron-injection process to ce-$MoS_2$ CB, the Fermi level of the semiconductor is increased, more comparable to the energy level for redox pair $H^+/H_2$, which decreases the overpotential of ce-$MoS_2$ for HER as we observed.

However, a central question that yet remains to be solved is how hot the electrons transferred from plasmonic metal to semiconductor (process III) can effectively compete with the electron−hole pair recombination (process II) in the metal. To achieve more efficient electrocatalytic activity, the electrons injection from the Au to $MoS_2$ should be faster than the recombination process (i.e., $k_{II} \gg k_{III}$). In the framework of the mechanism shown above, one would expect that the introduction of typical hole scavengers (HS), such as ethanol (EtOH), would reduce the possibility of electron−hole recombination and make the hot electrons display a prolonged lifetime. As shown in Figure 4C, with ethanol as HS, the HER onset potential of Au−$MoS_2$ is positively shifted by ca. 90 mV. The onset potential of Au−$MoS_2$ under laser irradiation with HS reaches as much as ca. −0.12 mV, which surpasses most of the state-of-art $MoS_2$ based materials (see Table S1 in the Supporting Information) and promises to bridge the gap with commercial Pt/C catalyst (Supporting Information Figure S10). Other HS (e.g., methanol (MeOH), glucose, fructose, ethylene glycol (EG) and glycerol) can also be employed to increase the HER activity (Figure 4D). This demonstrates the excellent versatility and the great potential of Au−$MoS_2$ hybrids for large-scale applications.

## CONCLUSION

From our findings, to achieve desired activity of catalysts toward HER, it is essential to improve the efficiency of light adsorption of Au rods, the electron−hole separation, and the transfer of intermediated hot electron from Au rods to $MoS_2$ active sites. This can be partially realized by removing the CTAB passivating layer covering the Au rods or completely wrapping Au rods with single-layer $MoS_2$. And further study can be conducted by tuning the plasmon resonance energy through the Au rods aspect ratio and doping $MoS_2$ with other elements. We find that plasmon-excited hot electrons injection mechanism is an efficient and promising strategy to improve the catalyst activity. Through electron injection, the carrier density of catalysts can be adjusted to match the energy level of interesting reactions, such as water splitting. Although still in its infancy, this field has witnessed considerable progress in high energy conversion. Moreover, the use of other plasmonic materials such as inexpensive copper and new semiconductors is proposed to extend the spectral range of light absorption and reduce the cost, achieving more applications in photocatalytic and electrocatalytic devices.

## ASSOCIATED CONTENT

### Supporting Information

The synthetic procedure of Au−$MoS_2$ nanosheets; image of dark-field electrochemical apparatus; SEM and TEM images; survey scans of XPS spectra; polarization curves; GC measurements of various samples; assessment of activation



DOI: 10.1021/jacs.5b01732
J. Am. Chem. Soc. 2015, 137, 7365−7370

energy ($E_a$); assessment of turnover frequency (TOF); table listing HER activities of $MoS_2$-based catalysts; UV−vis spectrum of Au rods; SPR scattering spectra of Au rods in Au/ITO and Au−$MoS_2$/ITO; $i$−$t$ curves of Au/ITO and Au-$MoS_2$/ITO. The Supporting Information is available free of charge on the ACS Publications website at DOI: 10.1021/jacs.5b01732.

## AUTHOR INFORMATION


### Corresponding Author

*xhxia@nju.edu.cn.


### Notes

The authors declare no competing financial interest.

## ACKNOWLEDGMENTS

This work is supported by grants from the National 973 Basic Research Program (2012CB933800), the National Natural Science Foundation of China (21275070, 21327902), the National Science Fund for Creative Research Groups (21121091).

## REFERENCES


(1) Dresselhaus, M. S.; Thomas, I. L. *Nature* **2001**, *414*, 332.
(2) Turner, J. A. *Science* **2004**, *305*, 972.
(3) Greeley, J.; Jaramillo, T. F.; Bonde, J.; Chorkendorff, I.; Norskov, J. K. *Nat. Mater.* **2006**, *5*, 909.
(4) Popczun, E. J.; McKone, J. R.; Read, C. G.; Biacchi, A. J.; Wiltrout, A. M.; Lewis, N. S.; Schaak, R. E. *J. Am. Chem. Soc.* **2013**, *135*, 9267.
(5) Kibsgaard, J.; Chen, Z.; Reinecke, B. N.; Jaramillo, T. F. *Nat. Mater.* **2012**, *11*, 963.
(6) Chen, W.-F.; Sasaki, K.; Ma, C.; Frenkel, A. I.; Marinkovic, N.; Muckerman, J. T.; Zhu, Y.; Adzic, R. R. *Angew. Chem., Int. Ed.* **2012**, *51*, 6131.
(7) Andreiadis, E. S.; Jacques, P. A.; Tran, P. D.; Leyris, A.; Chavarot-Kerlidou, M.; Jousselme, B.; Matheron, M.; Pécaut, J.; Palacin, S.; Fontecave, M.; Artero, V. *Nat. Chem.* **2013**, *5*, 48.
(8) Vrubel, H.; Hu, X. *Angew. Chem., Int. Ed.* **2012**, *51*, 12703.
(9) Jaramillo, T. F.; Jørgensen, K. P.; Bonde, J.; Nielsen, J. H.; Horch, S.; Chorkendorff, I. *Science* **2007**, *317*, 100.
(10) Hinnemann, B.; Moses, P. G.; Bonde, J.; Jørgensen, K. P.; Nielsen, J. H.; Horch, S.; Chorkendorff, I.; Nørskov, J. K. *J. Am. Chem. Soc.* **2005**, *127*, 5308.
(11) Xie, J.-F.; Zhang, J.-J.; Li, S.; Grote, F.; Zhang, X.-D.; Zhang, H.; Wang, R.-X.; Lei, Y.; Pan, B.-C; Xie, Y. *J. Am. Chem. Soc.* **2013**, *135*, 17881.
(12) Lukowski, M. A.; Daniel, A. S.; Meng, F.; Forticaux, A.; Li, L. S.; Jin, S. *J. Am. Chem. Soc.* **2013**, *135*, 10274.
(13) Li, Y.-G.; Wang, H.-L.; Xie, L.-M; Liang, Y.-Y.; Hong, G.-S.; Dai, H.-J. *J. Am. Chem. Soc.* **2011**, *133*, 7296.
(14) Huang, X.; Zeng, Z.-Y.; Bao, S.-Y.; Wang, M.-F.; Qi, X.-Y.; Fan, Z.-X.; Zhang, H.-X. *Nat. Commun.* **2013**, *4*, 1444.
(15) Kim, J.; Byun, S.; Smith, A. J.; Yu, J.; Huang, J. *J. Phys. Chem. Lett.* **2013**, *4*, 1227.
(16) Wu, K.; Rodríguez-Córdoba, W. E.; Yang, Y.; Lian, T. Q. *Nano Lett.* **2013**, *13*, 5255.
(17) Tanaka, A.; Hashimoto, K.; Kominami, H. *J. Am. Chem. Soc.* **2013**, *136*, 586.
(18) Silva, C. G.; Juárez, R.; Marino, T.; Molinari, R.; García, H. *J. Am. Chem. Soc.* **2010**, *133*, 595.
(19) Hoggard, A.; Wang, L.-Y.; Ma, L.-L.; Fang, Y.; You, G.; Olson, J.; Liu, Z.; Chang, W.-S.; Ajayan, P.-M.; Link, S. *ACS Nano* **2013**, *7*, 11209.
(20) Kong, B.; Tang, J.; Selomulya, C.; Li, W.; Wei, J.; Fang, Y.; Wang, Y.-C.; Zheng, G.-F.; Zhao, D.-Y. *J. Am. Chem. Soc.* **2014**, *136*, 6822.
(21) Yin, Z.-Y.; Chen, B.; Bosman, M.; Cao, X.-H.; Chen, J.-Z.; Zheng, B.; Zhang, H. *Small* **2014**, *10*, 3536.
(22) Kang, Y.-M.; Sina, N.; Liu, Z.; Bao, Y.-J.; Wang, Y.-M.; Zhu, X.; Naomi, J. H.; Peter, N.; Ajayan, P. M.; Lou, J.; Fang, Z.-Y. *Adv. Mater.* **2014**, *26*, 6467.
(23) Linic, S.; Christopher, P.; Ingram, D. B. *Nat. Mater.* **2011**, *10*, 911.
(24) Guo, Z.-R.; Gu, C.-R.; Fan, X.; Bian, Z.-P.; Wu, H.-F.; Yang, D.; Gu, N.; Zhang, J.-N. *Nanoscale Res. Lett.* **2009**, *4*, 1428.
(25) Ye, X.; Zheng, C.; Chen, J.; Gao, Y.; Murray, C. B. *Nano Lett.* **2013**, *13*, 765.
(26) Chou, S.-S.; De, M.; Kim, J.; Byun, S.; Dykstra, C.; Yu, J.; Huang, J.-X.; Dravid, V. P. *J. Am. Chem. Soc.* **2013**, *135*, 4584.
(27) Bertrand, P. A. *Phys. Rev. B* **1991**, *44*, 5745.
(28) Sreeprasad, T. S.; Nguyen, P.; Kim, N.; Berry, V. *Nano Lett.* **2013**, *13*, 4434.
(29) Chou, S. S.; Kaehr, B.; Kim, J.; Foley, B. M.; De, M.; Hopkins, P. E.; Huang, J.-X.; Brinker, C. J.; Dravid, V. P. *Angew. Chem., Int. Ed.* **2013**, *52*, 4160.
(30) Tributsch, H.; Bennett, J. C. *J. Electroanal. Chem. Interfacial Electrochem.* **1977**, *81*, 97.
(31) Voiry, D.; Yamaguchi, H.; Li, J.-W.; Silva, R.; Alves, D. C. B.; Fujita, T.; Chen, M.-W; Asefa, T.; Shenoy, V. B.; Eda, G.; Chhowalla, M. *Nat. Mater.* **2013**, *12*, 850.




DOI: 10.1021/jacs.5b01732
*J. Am. Chem. Soc.* 2015, 137, 7365−7370